Chinese Journal of Chemical Engineering 89 (2026) 230–239

Contents lists available at ScienceDirect

Chinese Journal of Chemical Engineering

journal homepage: www.elsevier.com/locate/CJChE

Full Length Article

Experimental investigation of biosurfactants on carbon dioxide hydrate formation

Gang Yue [1,*], Yu Liu [2], Yonghua Qin [1], Zongming Tian [1], Xuqiang Guo [3]

[1] Zhejiang Pharmaceutical University, Ningbo 315599, China
[2] Zhejiang Ningbo City Fenghua District Power Supply Bureau, Ningbo 315500, China
[3] China University of Petroleum-Beijing at Karamay, Karamay 834400, China

ARTICLE INFO

Article history:
Received 1 April 2025
Received in revised form
29 May 2025
Accepted 11 June 2025
Available online 16 September 2025

Keywords:
Biosurfactants
Hydrate
Kinetic
Model calculation

ABSTRACT

With the development of hydrate technology, more and more applications have been appeared in many areas. However, hydrate additive is always one research hotspot, it has attracted more and more attention. The influence of two biosurfactants on CO_2 hydrate formation process were investigated. Through the investigation of experiment research, rhamnolipid and sophorolipid had the promotion effect on CO_2 hydrate formation kinetics. Hydrate gas storage reached the maximum value 32.01 (volume ratio) and conversion ratio of water to hydrate was 19.42% when sophorolipid concentration was 0.05% (mass). Hydrate gas storage capacity reached the maximum value 31.22 (volume ratio) and conversion ratio of water to hydrate was 18.94% when rhamnolipid concentration was 0.05% (mass). Through the comparison of gas storage capacity and hydrate formation rate, sophorolipid had stronger promotion effect on CO_2 hydrate formation kinetics than rhamnolipid. It increased the depth of gas hydration reaction. CO_2 hydrate formation gas was carried out under the condition of constant temperature and volume. Hydration number was considered in the hydrate calculation process. Combined with hydrate formation kinetic theory of Chen–Guo model, the hydrated gas volume was compared with remaining volume of reactor. This model could calculate the change of CO_2 hydrate gas storage capacity over time. The calculated values of gas storage was in good agreement with experimental values. So this study has the better guiding function for relevant hydrate technology application.

1. Introduction

The massive consumption of fossil energy has led to increasing emission of carbon dioxide (CO_2). The resulting greenhouse effect has led to global temperature rise. Extreme weather, species extinction and other frequent problems, which have threatened the survival and development of human beings [1]. However, fossil fuels will still dominate the world's energy supply for a long time [2]. Therefore, the in-depth study of CO_2 capture and utilization and storage (CCUS) technology are of great significance [3,4]. Geological storage is one of important ways to realize CCUS technology [5]. The deep-sea hydrate storage of CO_2 (HCS) is one new geological storage technology, which could achieve long-term and stable storage by injecting CO_2 into strata or seabed sediments to form solid hydrate [6,7]. However, HCS technology still has a series of problems, such as long induc tion time of hydrate formation, strong randomness and slow growth of hydrate [8,9].

Gas hydrate is a non-stoichiometric cage-type crystal compound formed by gas and water molecules under certain temperature and pressure conditions. The hydrate is similar to ice [10]. Temperature scope of hydrate formation is 273.15–298.15 K and formation pressure of different gases has significant difference. In terms of hydrate gas storage capacity, each unit volume of hydrate could contain up to 180 times of gas volume. According to characteristics of large gas storage capacity of hydrate, it has good application in the prospect of gas storage and transportation [11]. For hydrate phase, van der Waals forces exists between molecules of gas and water. In order to generate the stable structure, good stability between gas and water molecular cages was required [12–14]. Scholars are looking for effective methods to enhance the hydrate formation actively. The key to popularization and application for HCS technology is to increase hydrate formation rate.

* Corresponding author. Zhejiang Pharmaceutical University, Zhejiang Ningbo, 315599, China.
E-mail address: yue3658@foxmail.com (G. Yue).

https://doi.org/10.1016/j.cjche.2025.06.032

Adding chemical additives is one common method to achieve the goal of rapid hydrate formation [15,16].

Hydrate additives mainly contained thermodynamic and kinetic additives [17]. In terms of hydrate thermodynamics study, it was mainly about additives influence on hydrate formation pressure. The mainly thermodynamic additives contained tetrahydrofuran (THF), cyclopentane (CP) and tetrabutylammonium bromide (TBAB) [18–20]. In terms of kinetics study, additives affect the hydrate nucleation rate, induction time and hydrate gas storage capacity. The kinetic additives mainly include surfactants, amino acids, starch [21,22], polymers and nanofluids [23,24]. The common surfactants were sodium dodecyl sulfate (SDS) and dodecyl trimethyl ammonium chloride(DTAC) [25–27]. Tryptophan, histidine and leucine were common amino acids hydrate additives [28–30]. Zhang *et al.* [31] carried out the experiment that the CO_2 liquefaction could promote the formation process of CO_2 hydrate in porous media within a certain range of liquefaction amount. Zhang *et al.* [32] also studied the influence of single grain sizes and porous media with grain gradatings of different mass ratios on the formation processes and storage characteristics of CO_2 hydrate. According to literature research and analysis, there existed many problems about hydrate technology, such as low hydrate generation rate, long induction time of hydrate nucleation, small gas storage capacity of hydrate, low mixture separation efficiency and so on. Therefore, hydrate additives with good performance need to be further screened and optimized from the perspective of energy conservation and environmental protection.

More and more scholars paid attention to selection of effective and environment friendly hydrate additives to develop hydrate related technologies. Biosurfactant is one kind of substance produced in metabolic process from plants or microorganisms and it has high surface activity. Compared with traditional chemical additives, biosurfactants has advantages in environmental protection and economical efficiency. The structure of biosurfactants contained some functional groups which were difficult to synthesize in chemical reactions. Biosurfactants were widely used in the area of food, soil remediation and underground oil extraction [33–35]. In view of good performance of biosurfactants on reducing solution surface activity, biosurfactants which contained rhamnolipid and sophorolipid were selected as hydrate additives to study their effects on hydration formation process. Rhamnolipid is one kind of surfactant that has been studied extensively at present. Rhamnolipid is an anionic surfactant mainly produced by buckthorn fruit and it has good water solubility. There are four types of rhamnolipids which contained RL1($Rha_2C_{10}C_{10}$), RL2 ($RhaC_{10}C_{10}$), RL3(Rha_2C_{10}) and RL4($RhaC_{10}$). Rhamnolipids were usually studied the mixture of two structures [36,37]. Sophorolipid is one kind of biosurfactant mainly in non-ionic form. Hydrophile-lipophile balance value of sophorolipid and rhamnolipid are 12 and 19 respectively. The critical micelle concentration of sophorolipid is low. The resulting micelle size of sophorolipid was large and interfacial activity was high. Related experiments about sophorolipid has not been investigated as hydrate additive. In this study, rhamnolipid and sophorolipid were used as hydrate additives to investigate their effects on gas hydrate formation. In this paper, RL and SL were used to stand for rhamnolipid and sophorolipid respectively.

2. Methods and Materials

2.1. Experiment preparation

2.1.1. Experimental material

The materials used in this experiment were listed in Table 1.

2.1.2. Experimental equipment

The experimental equipment was shown in Fig. 1.

The high-pressure reactor was manufactured by Jiangsu Haian Petroleum Research Instrument Co., Ltd. Its designed pressure was 25 MPa and its volume was 246 ml. The visual window was made of high-pressure glass. The hand pump was manufactured by Nantong Huaxing Petroleum Instrument Co., Ltd. The air bath model was WD2050, which was provided by Shanghai Experimental Instrument Factory Co., Ltd. Temperature control range of air bath was 253.15–403.15 K. The pressure sensor was provided by Fujian Shunchang Hongyun Precision Instrument Co., Ltd. and its uncertainty was ±0.02 MPa. The temperature sensor was provided by Hangzhou Meikang Automation Technology Co. Ltd. The temperature range was 223.15–523.15 K and its sensitivity was ±0.01 K.

2.2. Experimental

2.2.1. Calibration of experimental equipment

In order to ensure the accuracy of experimental results, it is necessary to evaluate the errors existing in experimental steps.

(1) Leak detection of experimental device: Leak detection was to check the air tightness of device. The various pipelines of experimental device were connected and the temperature and pressure controller were added. The device was filled with gas and its pressure was 5.0 MPa. The leakage point was detected by soapy water. When the leakage point was processed, air tightness was tested again. If gas pressure remained unchanged for 3 h, the air tightness of device was qualified.
(2) Calibration of temperature sensor: Put temperature sensor in water bath that could control the temperature. Temperature of water bath was controlled to adjust sensor reading and the temperature uncertainty was ±0.1 K.
(3) Pressure sensor calibration: Standard pressure gauge was used for comparison and calibration. The control pressure uncertainty was ±0.01 MPa.

2.2.2. Experimental steps for determination of hydrate formation pressure

The constant temperature pressure search method was used to determine hydrate formation pressure. The experimental steps were listed as follows.

Table 1
Experiment materials.

Material	CAS	Purity	Source
CO_2	124-39-9	99.99% (mol)	Beijing Yongsheng Gas Technology Co., Ltd.
Rhamnolipid(RL)	147858-26-2	95.0% (mass)	Xi 'an Ruijie Biological technology Co., Ltd.
Sophorolipid(SL)	148409-20-5	97.0% (mass)	Jiangxi Hengmao Biotechnology Co., Ltd.
Deionized water	7732-18-5	18 $m\Omega \cdot cm^{-1}$	Lab-made

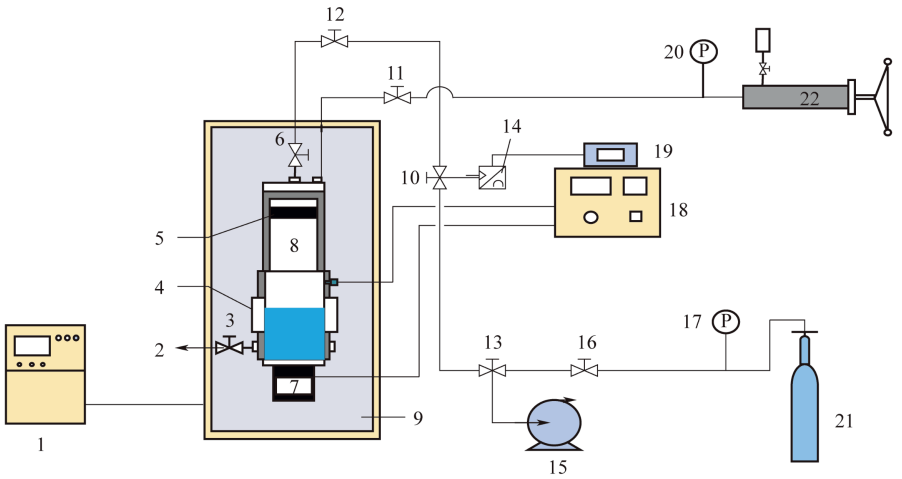

Fig. 1. Experiment equipment of hydrate phase equilibrium measurement. (1. Thermostatic control box; 2,3,6,10,11,12,13,16. Liquid or gas inlet and outlet valves; 4. Visual window; 5. Piston; 7,19. Stirring and temperature measuring device; 8. High-pressure reactor; 9. Air bath; 14,19. Pressure sensing and measurement systems; 15. Vacuum pump; 17,20. Pressure gauge; 21. Gas cylinders; 22. Manual pressure pump.)

(1) Liquid was injected into the reactor. The reactor was cleaned by deionized water. The pressure of reactor was pumped to negative with vacuum pump. The reactor was washed by deionized water at first, and then the working liquid was used to wash reactor three times. Finally, certain volume (80 ml) of reaction liquid was added to reactor.
(2) The reactor and pipeline system was purged with raw gas to ensure that there was no air in the experimental device. And then experimental gas was filled to achieve the predetermined pressure. The constant temperature air bath was opened and experimental temperature value was set. When temperature of reactor reached the predetermined value and remained stable for 1 h, it was considered that experimental temperature conditions had been satisfied.
(3) The stirring device was turned on and its speed was controlled at 1000 $r \cdot min^{-1}$. Hand pump was adjusted to increase gas pressure. The cold light source was turned on to observe gas hydrate formation process in reactor.
(4) If a large number of hydrate particles generated and the temperature raised substantially, hand pump was quickly adjusted to reduce gas pressure. A large number of hydrates dissolve and temperature dropped. When there were hydrate particles on liquid surface, the pressure and temperature remained unchanged and stable.
(5) If hydrate particles remained stable on the liquid surface for 3 h, the value was gas hydrate formation pressure at this temperature. If existence time of hydrate particles was short at this temperature, the hydrate melt and disappeared within 3 h and pressure should be adjusted again. The operation steps (3)–(5) should be repeated to measure hydrate formation pressure.
(6) When formation point of hydrate pressure at this temperature was determined, hand pump was adjusted to reduce gas pressure. Then the temperature was increased to dissolve hydrate particles completely. The next temperature point was adjusted and above steps were repeated to determine gas hydrate formation pressure at different temperature conditions.

2.2.3. Determination of measurement accuracy of experimental device

In order to further verify the accuracy of measurement data for experimental apparatus, formation pressure data of CO_2 hydrate in pure water was determined in this work. Experimental values were compared with literature results. The comparison was shown in Table 2 and Fig. 2.

Fig. 2 showed the comparison of CO_2 hydrate formation pressure in pure water between literature and experimental value. Compared with experimental value in this work, the relative average error of CO_2 formation pressure data with reference literature value 1 was 0.98% and the relative mean error of CO_2 hydrate formation pressure data in reference literature value 2 was 0.35%. It could be seen that error of experiment was small through the comparison. Accuracy of data measured by experimental device was high and the correctness of experimental operation step was verified.

2.2.4. Experimental Procedure

(1) First, high-pressure reactor was thoroughly cleaned three times with deionized water. And then it was cleaned three times with reaction liquid. Certain volume (90 ml) of working liquid was sucked into reactor by vacuum pump. The volume of reactor was 156 ml and the remaining volume could satisfy need for hydration.
(2) Use vacuum pump to make pipeline and reactor pressure to vacuum. And then it was purged three times with experimental gas to ensure that there was no air in the reactor. Then experimental gas was injected into reactor.
(3) Open the air bath to set temperature value. When reactor temperature reached the required experiment value and remained stable for 2 h. Stirrer was started and its rate was controlled at 1000 $r \cdot min^{-1}$. Meanwhile, change of pressure and temperature were recorded over time.
(4) When gas pressure in reactor did not drop any more, it indicated that hydration process has reached equilibrium. And then hydrated solution and remaining gas were emptied. Finally, the reactor was cleaned three times.

Table 2
Comparison of CO_2 hydrate formation pressure in pure water.

Literature value 1 [38]		Literature value 2 [39]		Experimental value	
Temperature/K	Pressure/MPa	Temperature/K	Pressure/MPa	Temperature/K	Pressure/MPa
273.9	1.37	274.3	1.42	273.9	1.39
275.2	1.56	275.5	1.63	275.5	1.63
276.1	1.76	277.6	2.11	276.1	1.75
278.9	2.42	279.1	2.55	279.1	2.57
280.7	3.13	280.6	3.12	280.7	3.15
282.0	3.84	281.5	3.51	281.5	3.50

(5) The experimental conditions of hydration process was changed and repeat above experimental steps. Changes of pressure and temperature were recorded over time. Finally, experimental data was organized and analyzed.

2.2.5. Experimental data processing

(1) Calculation of gas hydration consumption

The hydration process was carried out under constant temperature and volume. And total volume of gas remained constant. Change of pressure over time was recorded. The amount of substance in gas hydration process was calculated according to change of gas pressure. The calculation formula for gas consumption in hydrate phase was listed as follows:

$$\Delta n = \frac{P_1 V}{Z_1 RT} - \frac{P_2 V}{Z_2 RT} \tag{1}$$

In Eq. (1), P_1 and P_2 represented gas pressure at beginning and equilibrium of hydration process respectively. V represented volume of gas in hydration process, and the total volume of gas remained unchanged. Z represented gas compression factor and it was calculated by PR equation of state.

(2) The conversion ratio of water to hydrate

The conversion ratio of water to hydrate was calculated by following formula:

$$w = \frac{\Delta n_{H,\downarrow} \times n_{CO_2}}{n_{H_2O}} \tag{2}$$

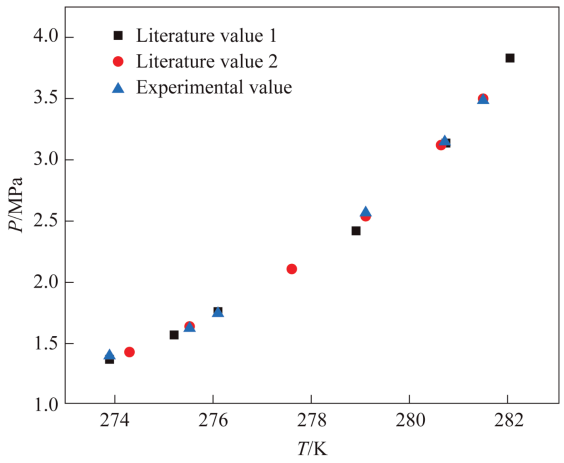

Fig. 2. Comparison of CO_2 hydrate formation pressure in pure water.

In Eq. (2), $\Delta n_{H,\downarrow}$ represented amount of gaseous substances in hydrate phase when hydration process reached equilibrium and calculated by Eq. (1), n_{H_2O} represented total amount of substances in water. n_{CO_2} represented size of hydration number.

CO_2 could form type I hydrate structure, which contained 46 water molecules, including six large pores and two small pores. If all pores were fully occupied, hydration number was 46/8. Joo *et al.* [40] described occupancy of CO_2 hydrate holes under appropriate pressure conditions. The hydration number was closely related to occupancy fraction of large and small holes.

The calculation formula of CO_2 hydration number was listed as follows:

$$n_{CO_2} = \frac{23}{3\theta_{L,CO_2} + \theta_{S,CO_2}} \tag{3}$$

In Eq. (3), occupancy of large pore and small pore of CO_2 and CH_4 hydrate could be obtained according to Ref. [41]. $\theta_{S,CO_2} = 0.81$ and $\theta_{L,CO_2} = 1.0$ were occupancy parameter values of small pore and large pore of CO_2 hydrate.

(3) Calculation of hydrate formation rate

Under the standard conditions, hydrate formation rate was calculated by following formula:

$$r = \frac{(\Delta n_{H,\downarrow})_t \Big/ n_{H_2O}}{t} \tag{4}$$

In Eq. (4), $\Delta n_{H,\downarrow}$ represented amount of gas substance in hydrate phase and its unit was mole. n_{H_2O} represented total amount of water in the system. t indicated hydration time. r represented the hydrate formation rate.

2.2.6. Kinetic model of CO_2 hydrate in biosurfactant solution

The influence of kinetics on CO_2 hydrate formation in two surfactant solutions had been explored. Addition of surfactant reduced solution surface tension and made resistance of gas molecules to enter into liquid phase smaller. Under the constant temperature and volume, With the increase of gas–liquid contact time, amount of hydrate increased and gas pressure gradually tended to stabilize at equilibrium pressure. The hydrate reaction reached equilibrium in the end. In this section, calculation model of CO_2 hydrate storage capacity in two surfactant solutions was established.

(1) Model study on kinetics of CO_2 hydrate formation

According to Chen–Guo hydrate model, process of gas hydrate formation were consist of two steps which were quasi-chemical reaction kinetic process and gas adsorption kinetic process. In the quasi-chemical reaction kinetics process of hydrate formation, molecular clusters were formed between gas

molecules in water phase and surrounding water molecules. Molecular clusters were unstable polyhedral structures, which were related to size of gas molecules. And the connecting holes formed by connection of molecular clusters were also one kind of holes. A certain stoichiometric basic hydrate was formed between gas molecules and water molecules. The second step was gas adsorption kinetic process. The basic hydrate generated in quasi-reaction kinetic process had certain holes and gas molecules would be adsorbed in connecting holes generated in previous process which led to non-stoichiometric property of hydrate. In the process of gas adsorption, hydrate pore diameter of connecting hole could only allow small gas molecules to pass through, but small gas molecules could not fully occupy connecting hole. Therefore, filling of gas molecules in hydrate connecting pores could be described by Langmuir adsorption theory.

The process of forming hydrate between CO_2 and water molecules could be described by the following formula [42]:

$$CO_2 + M\,H_2O \rightarrow CO_2 \cdot M\,H_2O \tag{5}$$

In Eq. (5), M represented hydration number. Type I hydrate structure was formed between CO_2 and water molecules, and hydration number was related to filling rate of large pores and small pores. The formula for calculating hydration number of type I hydrate was shown in Eq. (6):

$$M = \frac{23}{3\theta_L + \theta_S} \tag{6}$$

In Eq. (6), θ_L and θ_S represented occupancy of large pores and small pores respectively, which could be calculated by Langmuir adsorption theory.

The calculation of CO_2 gas consumption in hydrate phase was as follows:

$$\Delta n_{CO_2} = \frac{P_0 V_0}{Z_0 R T_0} - \frac{P_t V_t}{Z_t R T_t} \tag{7}$$

In Eq. (7), P and T represented temperature and pressure respectively, and V represented volume of gas in the reactor. Z represented gas compression factor, calculated from PR equation. R was gas constant 8.314 $J \cdot mol^{-1} \cdot K^{-1}$. The subscripts 0 and t indicated hydration at different time respectively. In the hydration formation process, volume of hydrate phase was different from volume of solution. Hydrate phase volume constantly changed with continuous entry of gas into hydrate phase. The volume of experimental gas in reactor changed with time which was defined as V_t. The calculation formula was listed as follows:

$$V_t = V_C - V_{F,H_2O} + V_{R,H_2O} - V_{Hydrate} \tag{8}$$

In Eq. (8), V_C represented total volume of reactor (246 ml), V_{F,H_2O} represented volume of solution (90 ml), V_{R,H_2O} represented volume of solution participating in hydration, $V_{Hydrate}$ represented volume of hydrate generated during hydration process, and subscript t represented hydration time. Volume of solution $V_{R,Water}$ that could participate in hydration was calculated as follows:

$$V_{R,H_2O} = M \times \Delta n_{CO_2} \times \nu_{H_2O}^{Liquid} \tag{9}$$

In Eq. (9), $\nu_{H_2O}^{Liquid}$ represented molar volume of liquid phase, and M represented hydration number, which could be obtained from Eq. (6). The specific calculation $\nu_{H_2O}^{Liquid}$ was listed as follows [43]:

$$\begin{aligned}\nu_{H_2O}^{Liquid} = 18.015 \times \Big\{1 - \left(1.0001 \times 10^{-2}\right) + \left(1.33391 \times 10^{-4}\right) \\ \times [1.8 \times (T - 273.15) + 32] + \left(5.50654 \times 10^{-7}\right) \\ \times [1.8 \times (T - 273.15) + 32]^2\Big\} \times 10^{-3}\end{aligned} \tag{10}$$

Table 3
Hydrate formation pressure of CO_2 in biological surfactants solutions.

Additive	Concentration /% (mass)	Temperature /K	Pressure /MPa	Additive	Concentration /% (mass)	Temperature /K	Pressure /MPa
H_2O		273.76	1.32			279.66	2.55
		275.45	1.61			281.67	3.34
		276.54	1.85			283.45	4.38
		277.69	2.08	SL	0.03	275.50	1.53
		278.77	2.42			277.98	2.08
		279.82	2.75			279.99	2.70
		280.95	3.21			281.80	3.50
RL	0.03	275.53	1.48			283.77	4.46
		277.68	1.98		0.05	275.87	1.57
		279.77	2.55			277.70	1.98
		281.96	3.53			279.83	2.62
		283.72	3.97			281.58	3.37
	0.05	275.52	1.49			283.76	4.43
		277.38	1.82		0.07	275.52	1.54
		279.24	2.28			277.34	1.93
		281.58	3.16			279.88	2.70
		283.68	4.09			281.92	3.52
	0.07	275.53	1.49			284.13	4.55
		277.45	1.86		0.09	275.96	1.59
		279.31	2.43			278.24	2.12
		281.25	3.18			279.64	2.54
		283.32	4.40			282.30	3.65
	0.09	275.71	1.54			284.17	4.43
		277.44	1.91				

In Eq. (10), units of T and $v_{H_2O}^{Liquid}$ were K and $m^3 \cdot kmol^{-1}$ respectively. Zhao *et al.* [44] proposed formula for calculating molar volume of type I empty base hydrate crystals which was function of temperature and pressure. The calculation formula was shown in Eq. (11):

$$v_{H_2O}^{MT}[I] = \left(11.835 + 2.217 \times 10^{-5}T + 2.242 \times 10^{-6}T^2\right)^3 \times \frac{10^{-30}N_A}{46} - 8.006 \times 10^{-9}P + 5.448 \times 10^{-12}P \quad (11)$$

In Eq. (11), N_A denoted Avogadro's constant which is $6.02214076 \times 10^{23}$; Assuming that molar volume of gas hydrate and empty hydrate crystal were equal, the formula for calculating volume of empty hydrate crystal was listed as follows:

$$V_{Hydrate} = M \times \Delta n_{CO_2} \times v_{H_2O}^{MT} \quad (12)$$

Gas storage capacity of hydrate was amount of gas stored per unit volume of hydrate under standard conditions. Calculation of CO_2 storage capacity in hydrate phase was listed as follows:

$$GS = \frac{V_0}{V_{Hydrate}} = \frac{\Delta n_{CO_2} RT_0/P_0}{V_{Hydrate}} \quad (13)$$

In Eq. (13), subscript 0 represented standard condition. $V_{Hydrate}$ represented hydrate volume when hydration process reached equilibrium.

(2) **Model calculation steps and flow chart of CO_2 hydrate gas storage capacity**

(1) Model calculation steps

① Input initial pressure P_0, temperature T, total volume of reactor V_C, volume of hydrated solution V_{F,H_2O}, gas pressure P_t at time t.

② The total volume of reactor and hydrated solution were used to calculate the remaining total volume of reactor.

③ According to formula, PR equation of state was used to calculate gas fugacity f_{gas}.

④ The hydration number M was calculated according to quasi-chemical reaction kinetics in Chen–Guo hydrate model and Langmuir adsorption theory.

⑤ The volume of water V_{R,H_2O} consumed in hydration process, volume of hydrate $V_{Hydrate}$ generated and gas consumption in the hydration process were calculated according to Eqs. (7), (9) and (12) respectively.

⑥ The volume of gas after hydration was calculated by Eq. (8) $V_t = V_C - V_{F,H_2O} + V_{R,H_2O} - V_{Hydrate}$.

⑦ The remaining volume of reactor was compared with volume of hydrated gas V_t.

⑧ The gas storage capacity of hydrate was calculated according to Eq. (13).

(3) Model calculation flow chart

The calculation flow of CO_2 hydrate storage capacity change over time was shown in Fig. 3.

3. Results and Discussion

3.1. CO_2 hydrate formation pressure in rhamnolipid and sophorolipid solution

In this section, hydrate formation pressure data of CO_2 gas in rhamnolipid and sophorolipid solutions were studied. The experimental results were shown in Table 3 and Fig. 4.

Fig. 4(a) showed the influence of rhamnolipid on CO_2 hydrate formation pressure. When concentration of rhamnolipid was 0.03% (mass), formation pressure of CO_2 hydrate decreases by 0.16 MPa compared with the value in pure water. When the concentration were 0.05% and 0.07% (mass), pressure dropped by 0.29 and 0.27 MPa. The thermodynamic promotion effect was the best. When the concentration of rhamnolipid was 0.09% (mass), the formation pressure of CO_2 hydrate was close to that of 0.03% (mass), and the formation pressure decreases by 0.18 MPa on average. Therefore, rhamnolipid had the promoting effect on CO_2

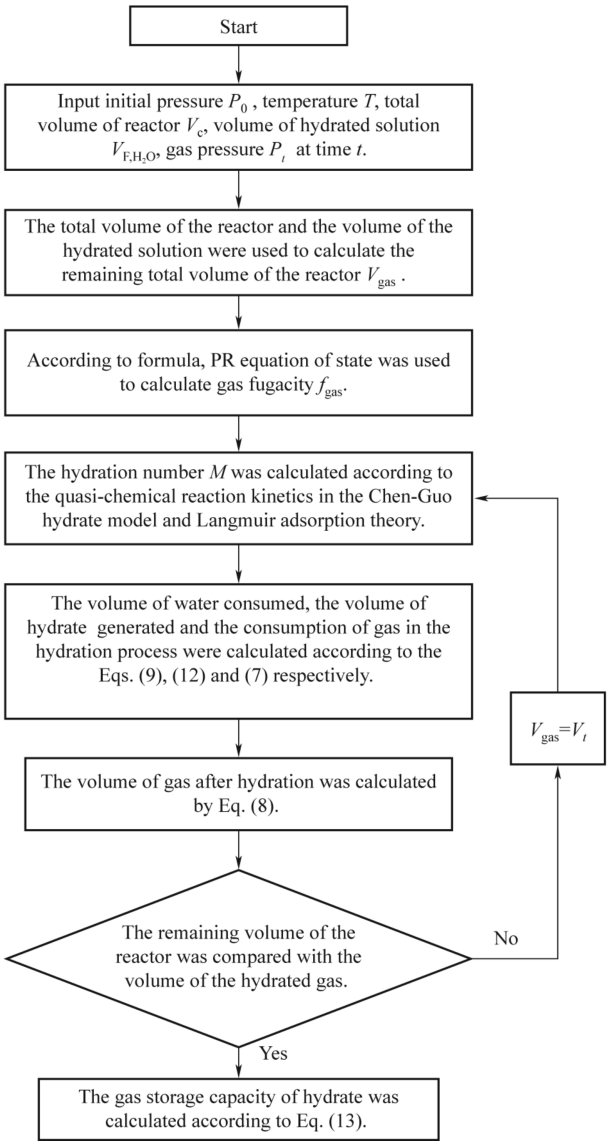

Fig. 3. Gas storage calculation process of CO_2 hydrate reaction.

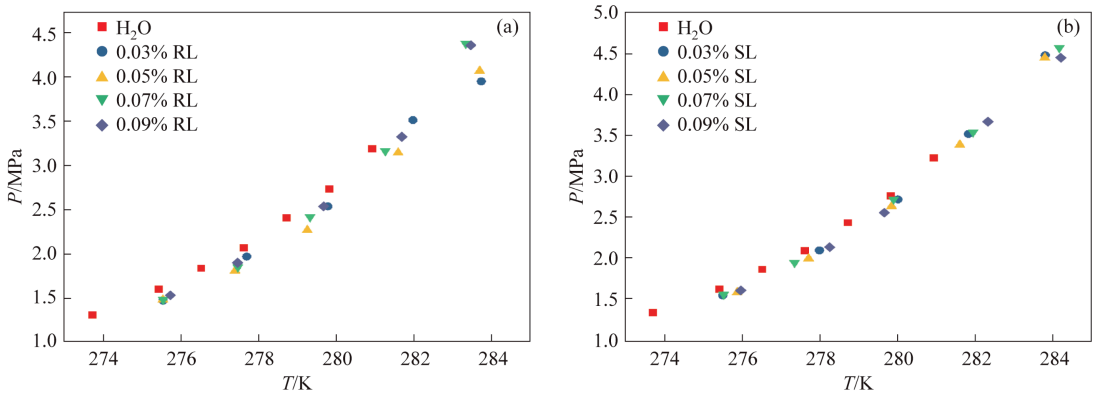

Fig. 4. Hydrate formation pressure of CO_2 in biological surfactant solutions: (a) RL, (b) SL.

hydrate formation pressure and thermodynamic promoting effect was obvious when the concentration was 0.05% (mass). Fig. 4(b) showed the influence of sophorolipid on CO_2 hydrate formation pressure. Compared with pure water, formation pressure of CO_2 hydrate decreased by 0.11 MPa when concentration of sophorolipid was 0.03% (mass). With the increase of concentration, promoting effect of sophorolipid on CO_2 hydrate formation pressure became weaker. When the concentration were 0.05% and 0.07% (mass), formation pressure of CO_2 hydrate decreased by 0.09 MPa on average. When concentration of sophorolipid was 0.09% (mass), formation pressure of CO_2 hydrate decreased by 0.13 MPa. Therefore, sophorolipid had thermodynamic promoting effect on formation pressure of CO_2 hydrate. Compared with rhamnolipid, sophorolipid had weaker thermodynamic promoting effect on formation pressure of CO_2 hydrate.

3.2. Effects of biosurfactants on the kinetics of CO_2 hydrate formation

In this section, hydrate formation kinetic data of CO_2 gas under different rhamnolipid and sophorolipid concentrations, temperature and initial intake pressure were measured as shown in Table 4. Comparison of experimental results under different conditions was shown in Fig. 5.

(1) Kinetics of CO_2 hydrate formation in rhamnolipid solution

This section studied the effect of different rhamnolipid concentrations, temperature and initial pressure on CO_2 hydrate formation. As can be seen from Fig. 5(a), compared with the results of CO_2 hydration process in pure water, growth rate of CO_2 hydrate reached the maximum value of 3.69×10^{-4} mol·mol^{-1}·min^{-1} when rhamnolipid concentration was 0.05% (mass). When rhamnolipid concentration increased from 0.03% to 0.07% (mass), and the gas storage capacity of CO_2 hydrate increased at first and then decreased. When concentration of rhamnolipid was 0.05% (mass), gas storage capacity of CO_2 hydrate reached maximum of 31.22 (volume ratio). When the concentration of rhamnolipid was 0.05% (mass), surface tension of the solution was minimal and the gas-liquid contact was sufficient, which was conducive to formation of CO_2 hydrate. Fig. 5(b) showed effects of different temperatures on CO_2 hydrate growth kinetics. With the decrease of temperature, gas storage capacity of CO_2 hydrate increases. When the pressure was 3.0 MPa, temperature dropped from 277.15 to 275.15 K, and gas storage capacity of CO_2 hydrate dropped from 24.37 to 34.73 (volume ratio), so low temperature was conducive to formation of CO_2 hydrate in rhamnolipid solution. Fig. 5(c) explored the influence of different initial pressure on CO_2 hydrate formation kinetics. With increase of pressure, consumption of CO_2 hydrate gas increased. At 276.15 K, hydrate formation pressure increased from 2.5 to 3.5 MPa and conversion rate of CO_2 hydrate increased from 9.31% to 19.73%. Fig. 5(b) and (c) described the change of gas pressure in the reactor. As for the crossing line in above figure, it

Table 4
CO_2 hydrate formation kinetics data in surfactant solutions.

Additive	Concentration /% (mass)	Temperature /K	Initial pressure /MPa	Balance pressure /MPa	T_{50} /min	Consumption /mol	Hydrate formation rate r	Gas storage capacity (volume ratio)	Percent conversion /%
H_2O	0	276.15	3.00	2.01	0.21	0.132	2.15×10^{-4}	26.28	15.94
RL	0.03	276.15	3.00	1.95	0.20	0.137	2.49×10^{-4}	27.32	16.57
	0.05	276.15	3.00	1.84	0.18	0.157	3.69×10^{-4}	31.22	18.94
	0.07	276.15	3.00	1.91	0.19	0.145	2.83×10^{-4}	28.88	17.55
	0.05	275.15	3.00	1.72	1.56	0.174	3.09×10^{-4}	34.73	21.07
	0.05	277.15	3.00	2.11	0.15	0.122	2.31×10^{-4}	24.37	14.73
	0.05	276.15	2.50	1.90	0.21	0.084	6.65×10^{-4}	16.65	10.11
	0.05	276.15	3.50	2.27	1.53	0.163	4.14×10^{-4}	32.52	19.73
SL	0.03	276.15	3.00	2.05	0.14	0.127	2.17×10^{-4}	25.24	15.31
	0.05	276.15	3.00	1.80	0.16	0.161	4.72×10^{-4}	32.01	19.42
	0.07	276.15	3.00	1.95	0.15	0.141	8.74×10^{-4}	28.10	17.05
	0.05	275.15	3.00	1.82	0.91	0.161	3.39×10^{-4}	32.12	19.49
	0.05	277.15	3.00	2.11	0.16	0.121	3.48×10^{-4}	24.11	14.63
	0.05	276.15	2.50	1.97	0.12	0.077	7.70×10^{-4}	15.35	9.31
	0.05	276.15	3.50	2.23	1.61	0.165	4.84×10^{-4}	32.78	19.89

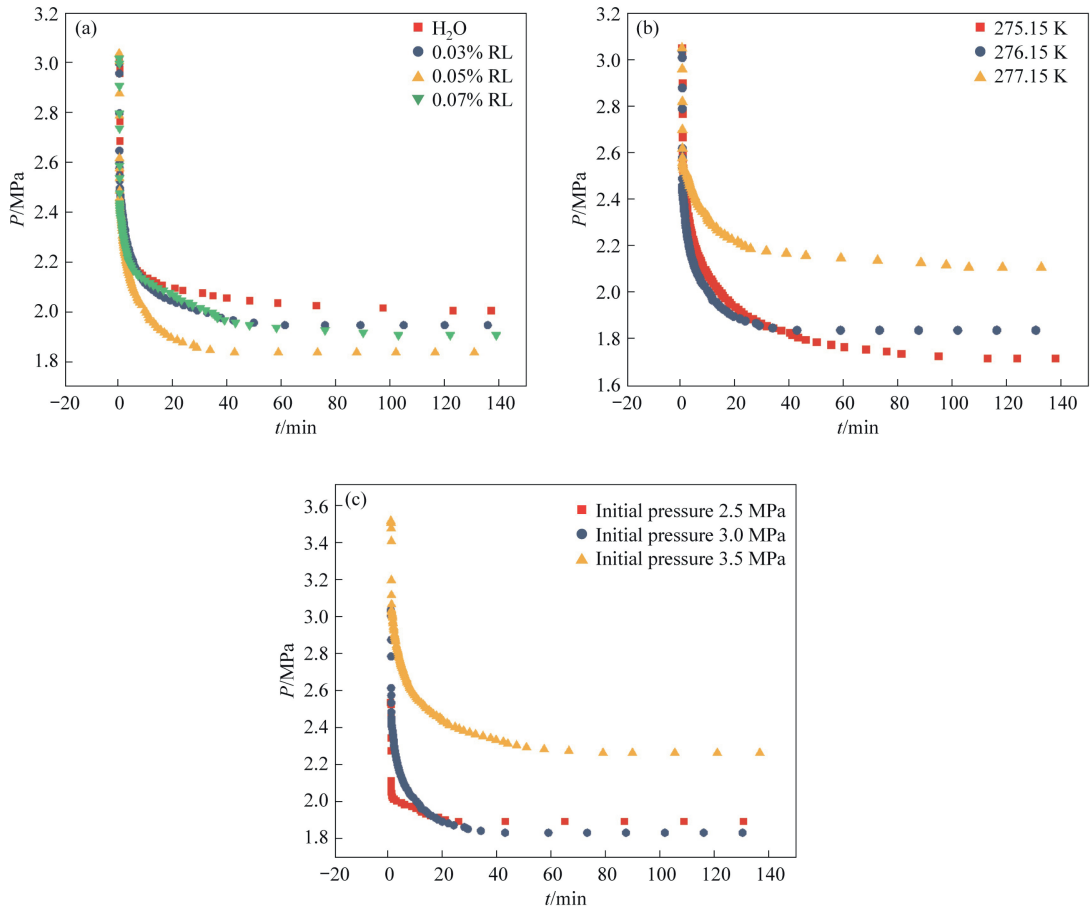

Fig. 5. CO_2 hydrate formation kinetics in rhamnolipid solution under different conditions: (a) concentration, (b) temperature, (c) feeding gas pressure.

was infected by the formed hydrate particles, stirred equipment and gas-liquid contact situation. So the gas pressure change curve in the reactor may had certain change. However, the final gas pressure had obvious rule when the hydrate reaction experiment was completed.

(2) CO_2 hydrate formation kinetics in sophorolipid solution

This section studied the influence of sophorolipid on CO_2 hydrate formation kinetics. Fig. 6(a) showed kinetics data of CO_2 hydrate formation in sophorolipid solution at different experimental concentrations (0.3%/0.5%/0.7% (mass)). Compared with pure water, when sophorolipid concentration increased from 0.03% to 0.07% (mass), gas storage capacity of CO_2 hydrate increased at first and then decreased. Hydrate formation rate increased from 2.17×10^{-4} to 8.74×10^{-4} $mol \cdot mol^{-1} \cdot min^{-1}$. When its concentration was 0.05% (mass), gas storage of hydrate reaches maximum value of 32.01 (volume ratio), and conversion rate of CO_2 hydrate was 19.42%. Under same temperature and pressure condition, conversion rate of CO_2 hydrate in rhamnolipid solution was 18.94%. Therefore, promotion effect of sophorolipid on gas storage of CO_2 hydrate was stronger than rhamnolipid. Fig. 6(b) showed effects of different temperatures on CO_2 hydrate growth kinetics in rhamnolipid solution. Gas storage capacity of CO_2 hydrate were 32.01 and 32.12 (volume ratio) respectively which was close at 275.15 and 276.15 K The storage capacity of CO_2 hydrate decreased to 24.11. Fig. 6(c) shows influence of different initial pressure on the kinetics of CO_2 hydrate formation in sophoripid solution. When gas pressure is 2.5 MPa, CO_2 hydrate storage capacity in rhamnolipid solution was 16.65 (volume ratio) which was higher than 15.35 (volume ratio) in sophorolipid solution. With increase of CO_2 pressure, gas storage capacity of CO_2 hydrate in sophoripid solution was higher than that of rhamnoipid, which were 32.78 and 32.52 (volume ratio) respectively. From analysis of hydrate formation rate and gas storage capacity, sophorolipid had stronger effect on CO_2 hydrate formation kinetics than rhamnolipid.

3.3. Storage capacity in rhamnolipid and sophorolipid solutions through hydrate formation kinetic model

Through the calculation of hydrate formation kinetic model, Fig. 7 showed the comparison between experimental and model values of CO_2 hydrate gas storage in rhamnolipid and sophorolipid solutions with different concentrations over time.

As can be seen from Fig. 7, model calculated value of gas storage was in good agreement with experimental value. Hydration of CO_2 gas was carried out under constant temperature and constant volume conditions. Hydration number was considered in calculation process. Combined with hydrate formation kinetic theory of Chen–Guo model, and then hydrated gas volume was compared with remaining volume of reactor. This model could better calculate change of CO_2 hydrate gas storage capacity over time.

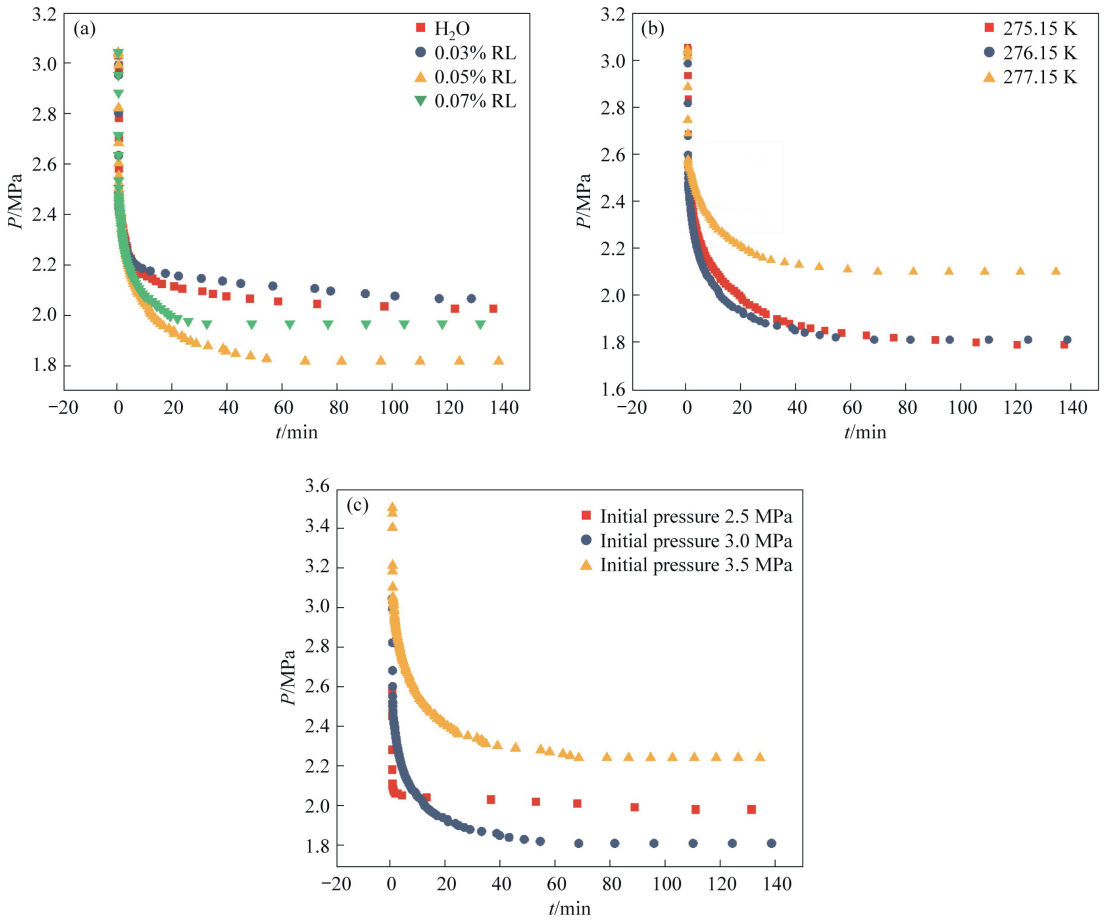

Fig. 6. CO_2 hydrate formation kinetics in SL solution under different conditions: (a) Concentration, (b) temperature, (c) initial pressure.

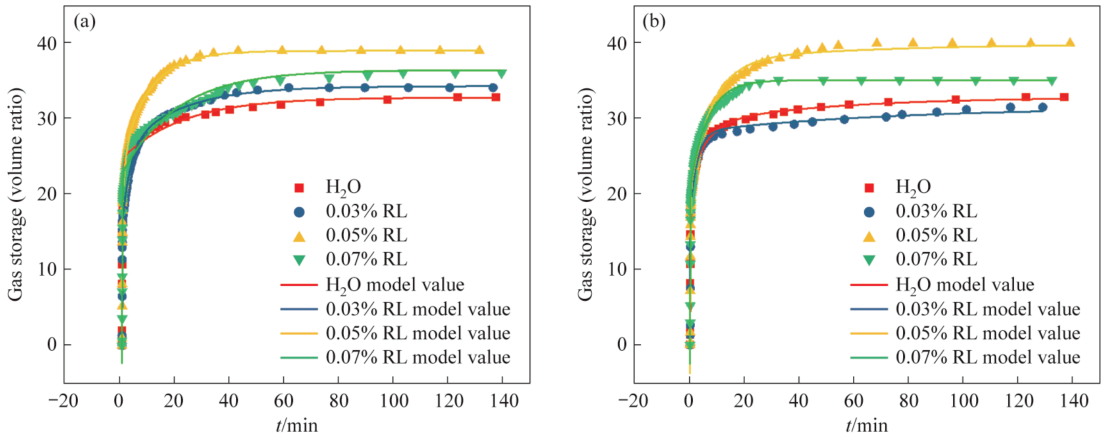

Fig. 7. Experiment and model values of CO_2 hydrate gas storage in different rhamnolipid (RL) (a) and sophorolipid (SL) (b) concentration solutions.

4. Conclusions

In this work, effect of two biosurfactants on CO_2 hydrate formation kinetics were investigated. In terms of biosurfactants rhamnolipid and sophorolipid, they had the promotion effect on CO_2 hydrate formation kinetics. When sophorolipid concentration was 0.05% (mass), gas hydrate storage reached the maximum value which was 32.01 (volume ratio), and the conversion ratio of water to hydrate was 19.42%. When the concentration of rhamnolipid was 0.05% (mass), gas storage capacity of hydrate reached the maximum 31.22 (volume ratio), and the conversion ratio of water to hydrate was 18.94%. Comparing the gas storage capacity and hydrate formation rate, sophorolipid had stronger effect on CO_2 hydrate formation kinetics than rhamnolipid, and it could increase the depth of gas hydrate reaction. The hydrate formation model of kinetics was established according with the relevant formula and theory in this work. Comparing with the experiment results, value of model calculated had the good consistency, so this model could make the application on hydrate formation kinetics in biogas additive solutions.

CRediT Authorship Contribution Statement

Gang Yue: Writing – original draft. Yu Liu: Supervision, Formal analysis. Yonghua Qin: Investigation. Zongming Tian: Investigation. Xuqiang Guo: Conceptualization.

Declaration of Competing Interest

The authors declare that they have no known competing financial interests or personal relationships that could have appeared to influence the work reported in this paper.

Acknowledgments

This work was financially supported by the Science Foundation of Zhejiang Pharmaceutical University Science Foundation of XIAO2024006, General project of Education Department of Zhejiang Province (2024116/Y202456535) and Fenghua District Science and Technology Association Natural Science Foundation Project 05, which were greatly acknowledged.

References

[1] Y. Kryzhanivskyy, V. Grudz, V. Zapukhliak, L. Poberezhny, Y. Melnychenko, R. Stasiuk, Prospects of utilizing unloaded parts of natural gas transmission pipelines in technologies of carbon dioxide capture and storage, *Procedia Struct. Integr.* 36 (2022) 370–377.
[2] F. Song, A. Sun, Carbon neutrality and renewable energy development in China, *China Econ. J.* 16 (2) (2023) 121–138.
[3] V. Eke, T. Sahu, K.K. Ghuman, M. Freire-Gormaly, P.G. O'Brien, A comprehensive review of life cycle assessments of direct air capture and carbon dioxide storage, *Sustain. Prod. Consum.* 55 (2025) 217–241.
[4] M. Ravichandran, T.T.A. Kumar, R. Dineshkumar, Carbon dioxide capture, sequestration, and utilization models for carbon management and transformation, *Environ. Sci. Pollut. Res.* 31 (44) (2024) 55895–55916.
[5] D. Segura, A. Cerepi, C. Loisy, J. Guélard, S. Noirez, C. Patrigeon, B. Garcia, Physicochemical behavior and impact of CO_2 and CH_4 plumes during gas-rich water leakage in a shallow carbonate freshwater aquifer, *Appl. Geochem.* 172 (2024) 106122.
[6] E.E. Kasala, J.J. Wang, W. Hussain, A. Majid, E.E. Nyakilla, Enhancing CO_2 hydrate formation and long-term stability in subseafloor saline sediments through integrated thermal and pressure management for effective CO_2 sequestration, *Appl. Energy* 377 (2025) 124680.
[7] S. Kim, S.H. Lee, Y.T. Kang, Characteristics of CO_2 hydrate formation/dissociation in H_2O + THF aqueous solution and estimation of CO_2 emission reduction by district cooling application, *Energy* 120 (2017) 362–373.
[8] Y.M. Kuang, W.Q. Li, Z.T. Lin, Y.P. Zheng, V.S.J. Craig, Experimental study on memory effect of gas hydrates: interaction between micronanobubbles and solute molecules, *J. Phys. Chem. C* 128 (38) (2024) 16237–16249.
[9] Y. He, F. Wang, Hydrate-based CO_2capture: kinetic improvement*via*-graphene-carried–SO_3^- and Ag nanoparticles, *J. Mater. Chem. A* 6 (45) (2018) 22619–22625.
[10] S. Kar, H. Kakati, A. Mandal, S. Laik, Experimental and modeling study of kinetics for methane hydrate formation in a crude oil-in-water emulsion, *Pet. Sci.* 13 (3) (2016) 489–495.
[11] V. Kumar Saw, G. Udayabhanu, A. Mandal, S. Laik, Methane hydrate formation and dissociation in the presence of silica sand and bentonite clay, *Oil Gas Sci. Technol. – Rev. IFP Energies Nouvelles* 70 (6) (2015) 1087–1099.
[12] R.T. Yan, H.F. Yu, D.H. Yang, H. Tang, Q. Zhang, Shear strength and pore pressure characteristics of methane hydrate-bearing soil under undrained condition, *Int. J. Hydrogen Energy* 48 (33) (2023) 12240–12256.
[13] V. Feyzi, V. Mohebbi, Experimental and modeling study of the kinetics of methane hydrate formation and dissociation, *Chin. J. Chem. Eng.* 29 (2021) 365–374.
[14] L. Kamiya, R. Kasai, S. Takeya, R. Ohmura, Phase equilibria and crystallographic structure of clathrate hydrate formed with carbon dioxide and cyclohexanone, *Fluid Phase Equilib.* 585 (2024) 114175.
[15] Y. Dai, X.X. Zhong, X. Jiang, S.L. Wang, Experiment of new additives effect on gas hydrate formation, *Energy Power Eng.* 6 (6) (2014) 133–141.
[16] Q. Nasir, H. Suleman, Y.A. Elsheikh, A review on the role and impact of various additives as promoters/inhibitors for gas hydrate formation, *J. Nat. Gas Sci. Eng.* 76 (2020) 103211.
[17] Z.X. Deng, S.S. Fan, Y.H. Wang, X.M. Lang, G. Li, Enhance hydrates formation with stainless steel fiber for high capacity methane storage, *Chin. J. Chem. Eng.* 50 (2022) 435–443.
[18] S.S. Fan, Q. Li, J.H. Nie, X.M. Lang, Y.G. Wen, Y.H. Wang, Semiclathrate hydrate phase equilibrium for CO_2/CH_4 gas mixtures in the presence of tetrabutylammonium halide (bromide, chloride, or fluoride), *J. Chem. Eng. Data* 58 (11) (2013) 3137–3141.
[19] A.H. Mohammadi, A. Eslamimanesh, D. Richon, Semi-clathrate hydrate phase equilibrium measurements for the CO_2+H_2/CH_4+*tetra-n*-butylammonium bromide aqueous solution system, *Chem. Eng. Sci.* 94 (2013) 284–290.
[20] K. Inkong, K. Jeemuang, S. Kulprathipanja, P. Rangsunvigit, Investigation of hydrate formation and stability of mixed methane-THF hydrates: effects of tetrahydrofuran concentration, *J. Oleo Sci.* 73 (9) (2024) 1159–1168.
[21] A. Kumar, T. Sakpal, D. Rajnish Kumar, Influence of low-dosage hydrate inhibitors on methane clathrate hydrate formation and dissociation kinetics, *Energy Technol.* 3 (7) (2015) 717–725.
[22] S. Maghsoodloo Babakhani, A. Alamdari, Effect of maize starch on methane hydrate formation/dissociation rates and stability, *J. Nat. Gas Sci. Eng.* 26 (2015) 1–5.
[23] Y.M. Song, F. Wang, G. Guo, S.J. Luo, R.B. Guo, Energy-efficient storage of methane in the formed hydrates with metal nanoparticles-grafted carbon nanotubes as promoter, *Appl. Energy* 224 (2018) 175–183.
[24] J. Yan, Y.Y. Lu, D.L. Zhong, Z.L. Zou, J.B. Li, Enhanced methane recovery from low-concentration coalbed methane by gas hydrate formation in graphite nanofluids, *Energy* 180 (2019) 728–736.
[25] A. Arora, S.S. Cameotra, R. Kumar, C. Balomajumder, A.K. Singh, B. Santhakumari, P. Kumar, S. Laik, Biosurfactant as a promoter of methane hydrate formation: thermodynamic and kinetic studies, *Sci. Rep.* 6 (2016) 20893.
[26] A. Kumar, G. Bhattacharjee, B.D. Kulkarni, R. Kumar, Role of surfactants in promoting gas hydrate formation, *Ind. Eng. Chem. Res.* 54 (49) (2015) 12217–12232.
[27] X.M. Zhang, M.J. Zhang, P.Y. Li, J.P. Li, Y.M. Wang, Q.B. Wu, Cooperative effect of surfactant and porous media on CO_2 hydrate formation and capacity of gas storage, *Fuel* 329 (2022) 125494.
[28] P. Naeiji, A. Arjomandi, F. Varaminian, Amino acids as kinetic inhibitors for tetrahydrofuran hydrate formation: experimental study and kinetic modeling, *J. Nat. Gas Sci. Eng.* 21 (2014) 64–70.
[29] G. Bhattacharjee, N. Choudhary, A. Kumar, S. Chakrabarty, R. Kumar, Effect of the amino acid l-histidine on methane hydrate growth kinetics, *J. Nat. Gas Sci. Eng.* 35 (2016) 1453–1462.
[30] C.B. Bavoh, B. Lal, H. Osei, K.M. Sabil, H. Mukhtar, A review on the role of amino acids in gas hydrate inhibition, CO_2 capture and sequestration, and natural gas storage, *J. Nat. Gas Sci. Eng.* 64 (2019) 52–71.
[31] X.M. Zhang, J.X. Wang, H.J. Yang, J.P. Li, Y.H. Li, Q.B. Wu, Formation and storage characteristics of CO_2 hydrate in porous media: effect of liquefaction amount on the formation rate, accumulation amount, *Appl. Therm. Eng.* 214 (2022) 118747.
[32] X.M. Zhang, P.Y. Li, H.B. Song, H. Sun, W.Q. Cui, J.P. Li, Q.B. Wu, P. Zhang, Experimental study on the formation and storage characteristics of CO_2 hydrate under condition of grain gradating: influence of different particle sizes and ratios, *Geoenergy Sci. Eng.* 249 (2025) 213794.
[33] C.S. Madankar, A. Meshram, Review on classification, physicochemical properties and applications of microbial surfactants, *Tenside Surfactants Deterg.* 59 (1) (2022) 1–16.
[34] A. Karthick, B. Roy, P. Chattopadhyay, A review on the application of chemical surfactant and surfactant foam for remediation of petroleum oil contaminated soil, *J. Environ. Manag.* 243 (2019) 187–205.
[35] G. Soberón-Chávez, R. Hausmann, E. Déziel, Editorial: biosurfactants: new insights in their biosynthesis, production and applications, *Bioeng Biotechnol* 9 (2021) 769899.
[36] M. Irfan-Maqsood, M. Seddiq-Shams, Rhamnolipids: well-characterized glycolipids with potential broad applicability as biosurfactants, *Ind. Biotechnol.* 10 (4) (2014) 285–291.
[37] Z.` Samsu, F.N. Jeffry, W.N.A.N. Wan, A.R. Azizan, Preliminary characterization and antimicrobial activity of crude biosurfactant extract from potential bacterial isolates, *Mater. Today Proc.* 31 (2020) A72–A78.
[38] J. Lee, J.W. Kenney III, Clathrate hydrates, in: Solidification, IntechOpen, 2018.
[39] S. Ovalle, C. Martinez, J.G. Beltran, Phase equilibria of hydrates from ternary mixtures of methane + ethane + propane and methane + propane + carbon dioxide, *Can. J. Chem. Eng.* 101 (2) (2023) 651–656.
[40] S. Joo, S. Kwak, Y. Yoon, Effect of H_2 enrichment ratio and $N2/CO_2$ dilution on swirl-stabilized partially premixed $H2/CH_4/C_3H_8$ SNG combustion, *Int. J. Hydrogen Energy* 45 (55) (2020) 31255–31267.
[41] R.H. Temperton, M.I. Smith, J.S. Sharp, Mechanical vibrations of pendant liquid droplets, *Eur. Phys. J. E* 38 (7) (2015) 79.
[42] H. Sojoudi, M.R. Walsh, K.K. Gleason, G.H. McKinley, Investigation into the formation and adhesion of cyclopentane hydrates on mechanically robust vapor-deposited polymeric coatings, *Langmuir* 31 (22) (2015) 6186–6196.
[43] L.S. Wang, J. Gmehling, Improvement of SRK equation of state for vapor-liquid equilibria of petroleum fluids, *AIChE J.* 45 (5) (1999) 1125–1134.
[44] H.N. Zhao, Z.B. Fang, H.B. Jing, J.Q. Liu, Modeling vapor-liquid phase equilibria of hydrogen sulfide and water system using a cubic EOS-GEX model, *Fluid Phase Equilib.* 484 (2019) 60–73.